Supporting Information Appendix

LDH Inhibition Synergizes with IL-21 to Promote CD8$^+$ T Cell Stemness and Antitumor Immunity

Dalton Hermans, Sanjivan Gautam, Juan C. García-Cañaveras, Daniel Gromer, Suman Mitra, Rosanne Spolski, Peng Li, Stephen Christensen, Rosa Nguyen, Jian-Xin Lin, Jangsuk Oh, Ning Du, Sharon Veenbergen, Jessica Fioravanti, Risa Ebina-Shibuya, Christopher Bleck, Leonard M. Neckers, Joshua D. Rabinowitz, Luca Gattinoni, Warren J. Leonard

Contains:

www.pnas.org/cgi/doi/10.1073/pnas.1920413117

Table S1. List of genes from RNA-Seq analysis in pre-activated $CD8^+$ T cells, either no treatment or treated with IL-2, IL-21, IL-2+LDHi, or IL-21+LDHi. **Tab 1**: Gene expression for all genes in cells receiving NC, IL-2, IL-21, IL-2+LDHi, or IL-21+LDHi. Two biological replicates were analyzed. **Tab 2**: Differentially expressed genes for IL-2 vs. NC. **Tab 3**: Differentially expressed genes for IL-21 vs. NC. **Tab 4**: Differentially expressed genes for IL-2+LDHi versus IL-2. **Tab 5**: Differentially expressed genes for IL-21+LDHi versus IL-21. **Tab 6**: Differentially expressed genes for IL-2 versus IL-21. **Tab 7**. Differentially expressed genes for IL-2+LDHi versus IL-21+LDHi. **Tab 8**: Gene expression for metabolism genes, corresponding to **Fig. 1H**. **Tab 9**: Gene expression for metabolism genes, corresponding to **Fig. 2H**. **Tab 10**: Gene expression for cell cycle genes, corresponding to **Fig. S3G**.

Figure S1

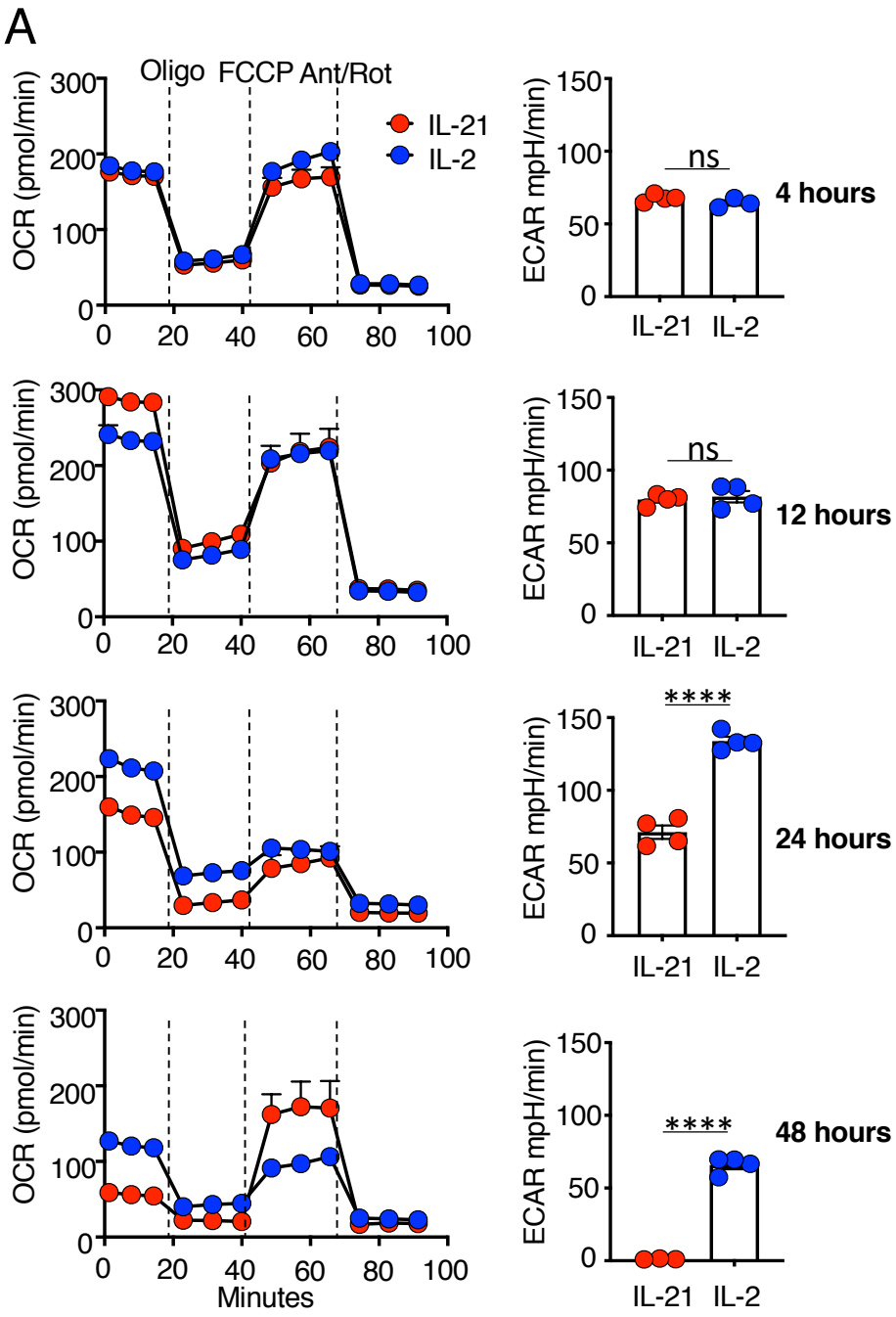
A
Oligo FCCP Ant/Rot
IL-21
IL-2
OCR (pmol/min)
ECAR mpH/min)
ns
4 hours
12 hours
****
24 hours
48 hours
IL-21 IL-2
Minutes

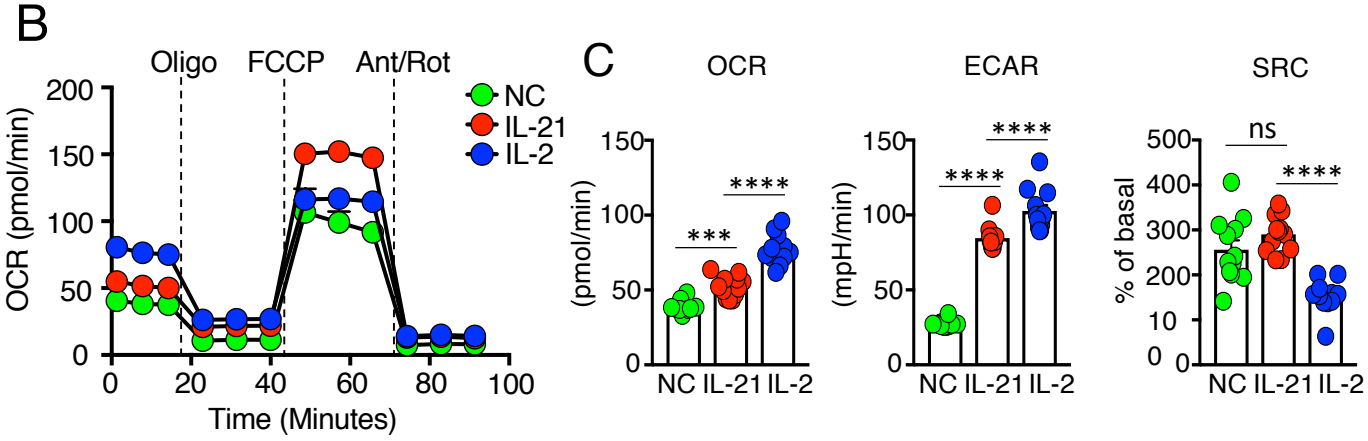
B
Oligo FCCP Ant/Rot
NC
IL-21
IL-2
OCR (pmol/min)
Time (Minutes)
C
OCR
ECAR
SRC
***
****
(mpH/min)
% of basal
ns
NC IL-21 IL-2

Fig. S1. Distinctive metabolic effects of IL-21 and IL-2 on mouse and human $CD8^+$ T cells. **(A)** OCR (left panels) and ECAR (right panels) induced by IL-21 and IL-2 in mouse $CD8^+$ T cells. The OCRs are shown for $CD8^+$ T cells treated with IL-21 (red) or IL-2 (blue) following treatment with oligomycin, FCCP, and antimycin A/rotenone. Cells were activated with anti-CD3 + anti-CD28 for 48 h and then stimulated with cytokine for 4, 12, 24, or 48 h, as indicated. This experiment is representative of 3 independent experiments. (**B**) Seahorse experiment showing OCRs for human $CD8^+$ T cells treated with no cytokine (green), IL-21, or IL-2, following treatment with oligomycin, FCCP, and antimycin A/rotenone. (**C**) Bar graphs indicate basal OCR measurements (left), basal ECAR measurements (middle), and SRC (right), as measured from Seahorse assays in (**B**).

Figure S2

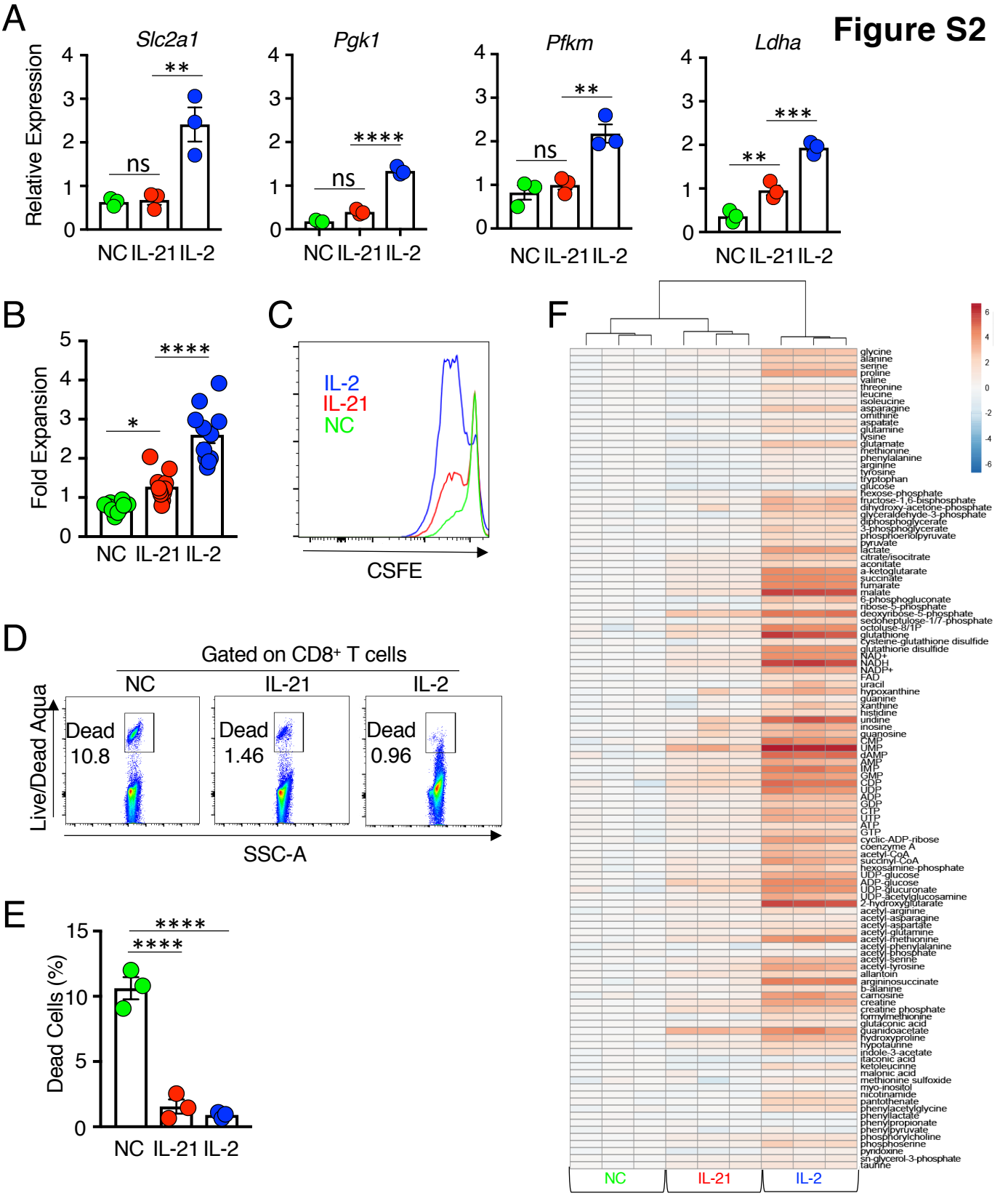
A
Slc2a1
Pgk1
Pfkm
Ldha
Relative Expression
NC IL-21 IL-2
B
Fold Expansion
C
IL-2
IL-21
NC
CSFE
D
Gated on CD8⁺ T cells
NC
IL-21
IL-2
Live/Dead Aqua
Dead 10.8
Dead 1.46
Dead 0.96
SSC-A
E
Dead Cells (%)
F
glycine
alanine
serine
proline
valine
threonine
leucine
isoleucine
asparagine
ornithine
aspatate
glutamine
lysine
glutamate
methionine
phenylalanine
arginine
tyrosine
tryptophan
glucose
hexose-phosphate
fructose-1,6-bisphosphate
dihydroxy-acetone-phosphate
glyceraldehyde-3-phosphate
diphosphoglycerate
3-phosphoglycerate
phosphoenolpyruvate
pyruvate
lactate
citrate/isocitrate
aconitate
a-ketoglutarate
succinate
fumarate
malate
6-phosphogluconate
ribose-5-phosphate
deoxyribose-5-phosphate
sedoheptulose-1/7-phosphate
octoluse-8/1P
glutathione
cysteine-glutathione disulfide
glutathione disulfide
NAD+
NADH
NADP+
FAD
uracil
hypoxanthine
guanine
xanthine
histidine
uridine
inosine
guanosine
CMP
UMP
dAMP
AMP
IMP
GMP
CDP
UDP
ADP
GDP
CTP
UTP
ATP
GTP
cyclic-ADP-ribose
coenzyme A
acetyl-CoA
succinyl-CoA
hexosamine-phosphate
UDP-glucose
ADP-glucose
UDP-glucuronate
UDP-acetylglucosamine
2-hydroxyglutarate
acetyl-arginine
acetyl-asparagine
acetyl-aspartate
acetyl-glutamine
acetyl-methionine
acetyl-phenylalanine
acetyl-phosphate
acetyl-serine
acetyl-tyrosine
allantoin
argininosuccinate
b-alanine
carnosine
creatine
creatine phosphate
formylmethionine
glutaconic acid
guanidoacetate
hydroxyproline
hypotaurine
indole-3-acetate
itaconic acid
ketoleucinne
malonic acid
methionine sulfoxide
myo-inositol
nicotinamide
pantothenate
phenylacetylglycine
phenyllactate
phenylpropionate
phenylpyruvate
phosphorylcholine
phosphoserine
pyridoxine
sn-glycerol-3-phosphate
taurine
NC
IL-21
IL-2
G
Glucose Uptake
MFI x 10³
H
Glucose
Intensity (a.u. x 10⁶)
I
Pyruvate
Intensity (a.u. x 10⁷)
J
NC
IL-21
IL-2
Phospho-PDH
β-Actin

Fig. S2. Differential effects of IL-2 versus IL-21 on expression of metabolism-related genes, proliferation, cellular viability are consistent with metabolomic profiling. (**A**) mRNA expression levels by qRT-PCR of *Slc2a1, Pgk1*, *Pfkm,* and *Ldha* in mouse T cells treated with no cytokine, IL-2, or IL-21. Measurements were analyzed using the ΔΔCq method of quantification. (**B-E**) Proliferation and viability of $CD8^+$ T cells treated with IL-21 versus IL-2. (**B**) Cellular expansion *in vitro* following 48 h of treatment with no cytokine (green), IL-21 (red), or IL-2 (blue). Measurements were pooled from 4 independent experiments. (**C**) Flow cytometry graph of CFSE staining for activated cells treated for 48 h with no cytokine, IL-21, or IL-2. (**D**) SSC-A versus Live/Dead Aqua flow cytometry graphs gated on $CD8^+$ T cells; samples are from cells stimulated with no cytokine, IL-21, or IL-2. (**E**) Flow cytometry-derived percentage of dead cells following 48 h of treatment with no cytokine, IL-21, or IL-2. (**F-J**) Metabolomic repertoires in cells treated with no cytokine (NC), IL-21, or IL-2, revealing that IL-2 induces LDHA and regulates the fate of pyruvate. (**F**) Heatmap of differential concentrations of cellular metabolites expressed as $\log_2$FC using NC as reference (n=3). (**G-I**) FACS measurement of glucose uptake (**G**) and LC-MS-based analysis of intracellular glucose (**H**) and pyruvate (**I**) in mouse T cells pre-activated with anti-CD3 + anti-CD28 for 48 h and then treated with no cytokine, IL-21, or IL-2. (**J**) Western blot of phosphorylated PDH (upper panel) and β-actin loading control (lower blot).

Figure S3

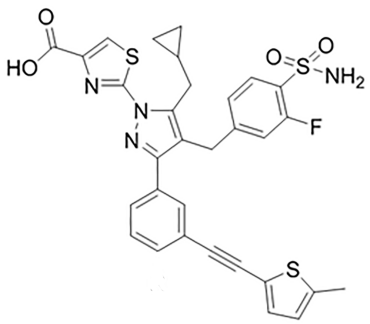
A
HO
O
N
S
N
N
O
S
O
NH2
F
S

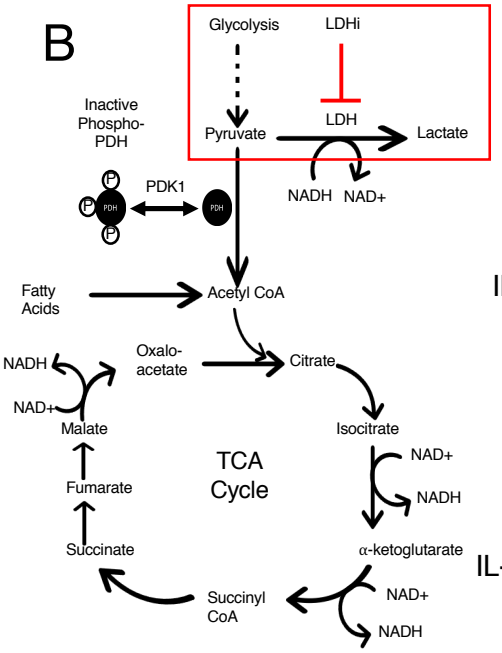
B
Glycolysis
LDHi
Inactive
Phospho-
PDH
Pyruvate
LDH
Lactate
NADH
NAD+
PDK1
Fatty
Acids
Acetyl CoA
NADH
NAD+
Oxalo-
acetate
Citrate
Malate
Isocitrate
TCA
Cycle
NAD+
NADH
Fumarate
Succinate
α-ketoglutarate
Succinyl
CoA
NAD+
NADH

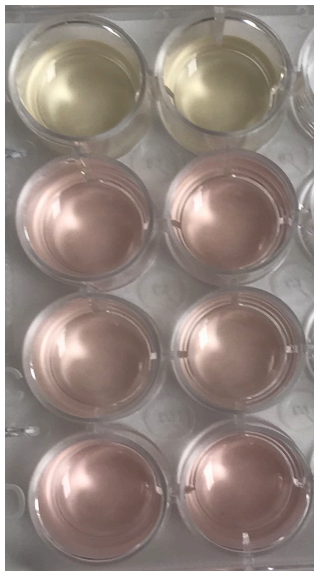
C
IL-2
IL-2+LDHi
IL-21
IL-21+LDHi

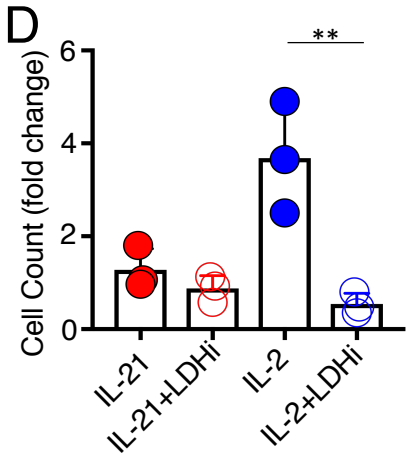
D
Cell Count (fold change)
0
2
4
6
**
IL-21
IL-21+LDHi
IL-2
IL-2+LDHi

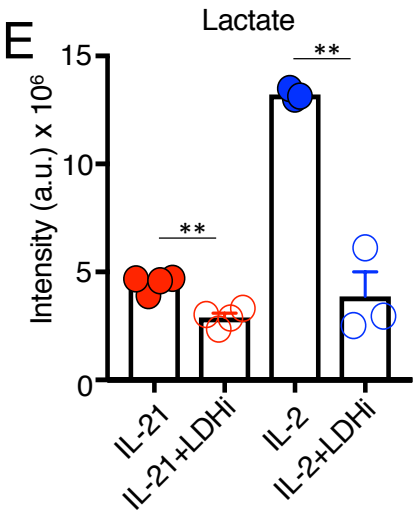
E
Lactate
Intensity (a.u.) x 10⁶
0
5
10
15
**
**
IL-21
IL-21+LDHi
IL-2
IL-2+LDHi

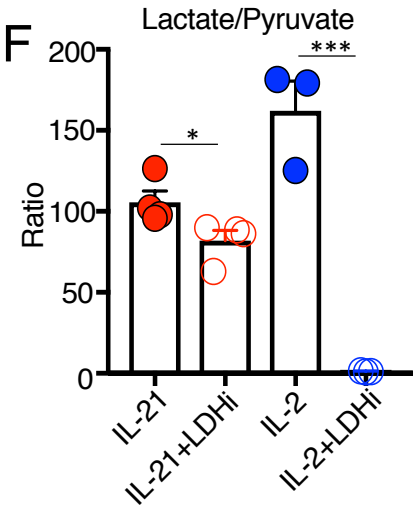
F
Lactate/Pyruvate
Ratio
0
50
100
150
200
*
***
IL-21
IL-21+LDHi
IL-2
IL-2+LDHi

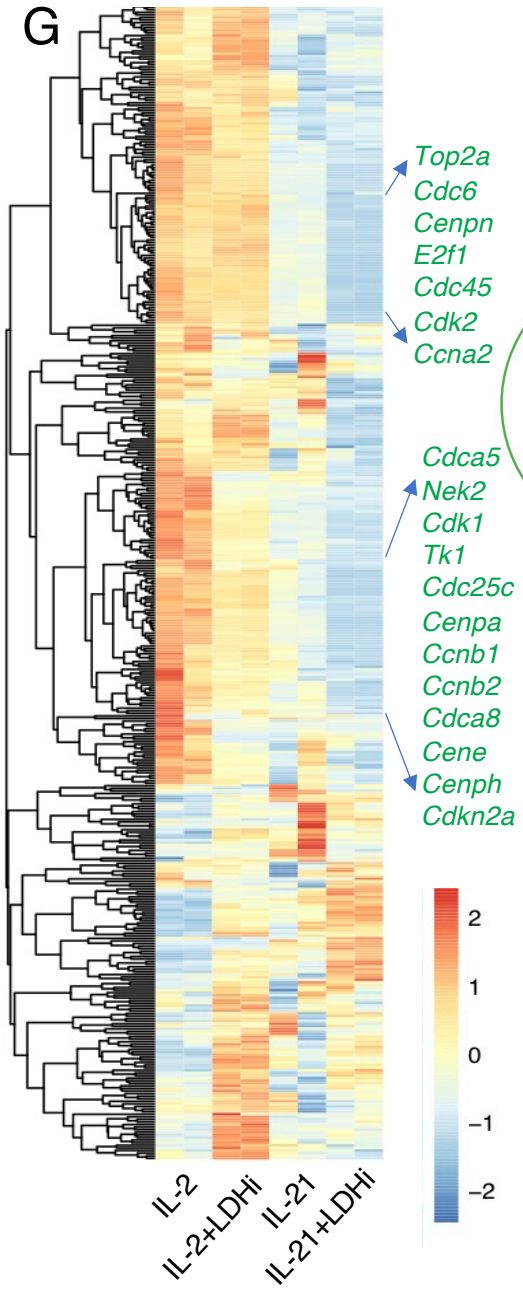
G
Top2a
Cdc6
Cenpn
E2f1
Cdc45
Cdk2
Ccna2
Cdca5
Nek2
Cdk1
Tk1
Cdc25c
Cenpa
Ccnb1
Ccnb2
Cdca8
Cene
Cenph
Cdkn2a
2
1
0
−1
−2
IL-2
IL-2+LDHi
IL-21
IL-21+LDHi

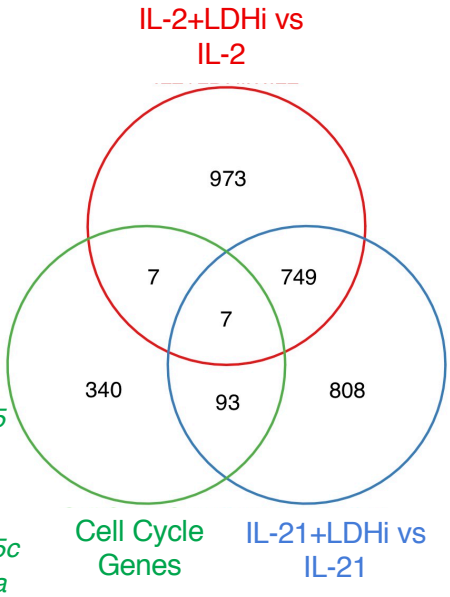
IL-2+LDHi vs
IL-2
973
7
749
7
340
93
808
Cell Cycle
Genes
IL-21+LDHi vs
IL-21

Fig. S3. Increased lactate production and lactate/pyruvate ratio in IL-2 treated cells and effects of an LDH inhibitor on IL-2- versus IL-21-regulated genes. (**A**) Structure of the LDH inhibitor, here denoted LDHi (NCI-737; $C_{31}H_{26}FN_4O_4S_3$), IUPAC name 2-(5-(cyclopropylmethyl)-4-(3-fluoro-4-sulfamoylbenzyl)-3-(3-((5-methylthiophen-2-yl)ethynyl)phenyl)-1H-pyrazol-1-yl)thiazole-4-carboxylic acid (26). (**B**) Schematic of metabolic pathways and regulatory genes important for pyruvate access to the TCA cycle and fermentation. The region boxed in red shows the effect of LDHi. (**C**) Greater acidity of $CD8^+$ T cells treated with IL-2 is reversed by LDHi. Photograph of cell media color after activated $CD8^+$ T cells underwent 48 h stimulation with IL-2, IL-2+LDHi, IL-21, or IL-21+LDHi. (**D-F**) Cell numbers (**D**), lactate level (**E**), and lactate/pyruvate ratio (**F**) for cells treated with IL-21, IL-21+LDHi, IL-2, or IL-2+LDHi. (**G)** Differentially expressed cell cycle genes in cells treated with IL-2, IL-2+LDHi, IL-21, or IL-21+LDHi. Left panel, RNA-Seq heatmap); the color scale indicates the fold induction. Each stimulation was performed in duplicate. Listed are some of the differentially-expressed cell cycle related genes. Right panel, Venn diagram showing overlap of cell cycle related genes versus genes differentially expressed genes for cells treated with IL-2 versus IL-2+LDHi as well as IL-21 versus IL-21+LDHi.

Figure S4

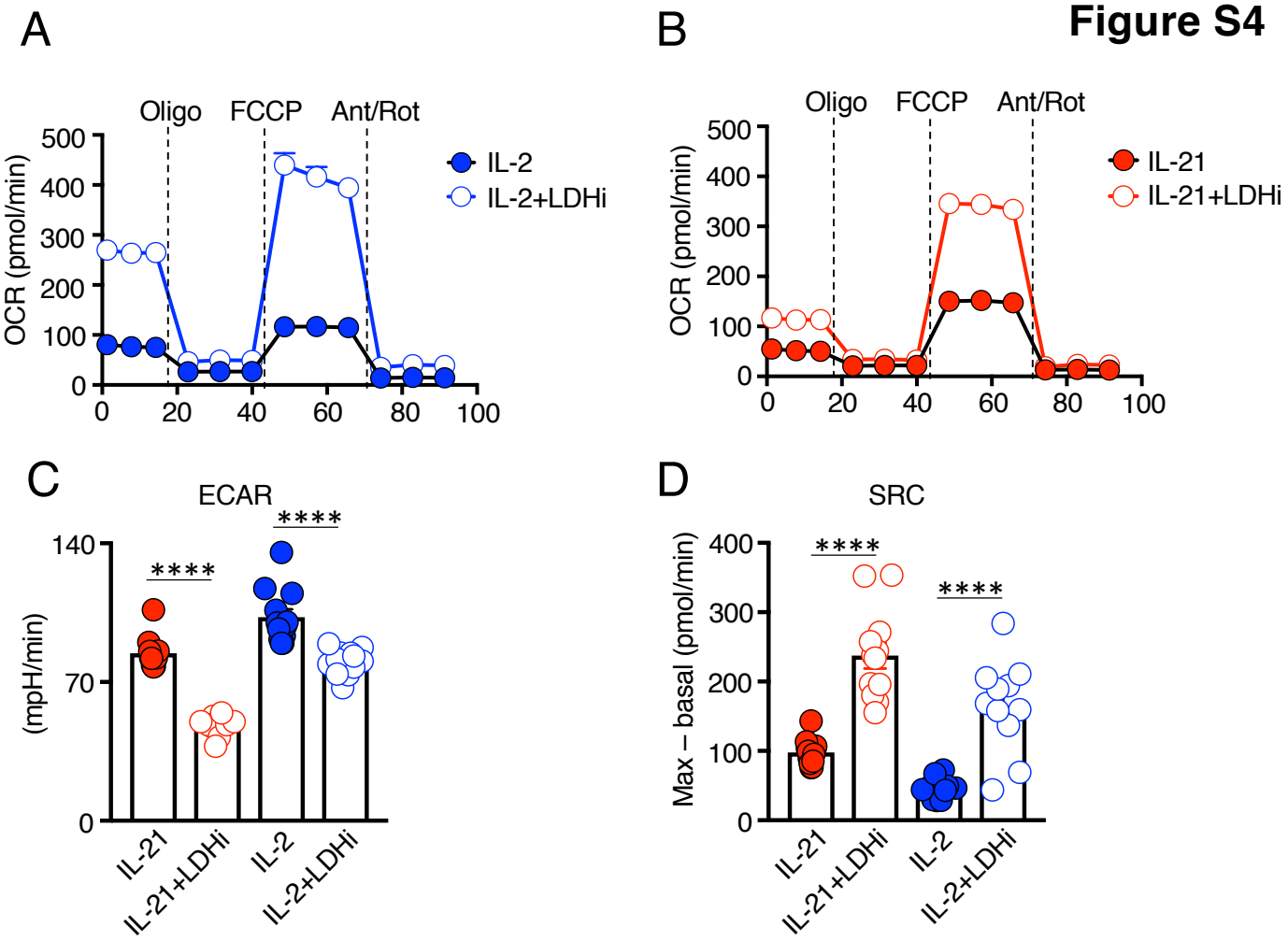

Fig. S4. Metabolic effects of LDHi on IL-2- and IL-21-stimulated human CD8$^+$ T cells. (**A and B**) OCRs for human CD8$^+$ T cells treated with **(A)** IL-2 (solid blue) or IL-2+LDHi (open blue) and **(B)** IL-21 (solid red) or IL-21+LDHi (open red). (**C and D**) ECAR (**C**) and SRC (**D**) measurements from Seahorse graphs in **(A)** and **(B)**.